Multi-vector Energy Systems for a Fragmented Grid: Thermodynamic and Constructal Insights

Boris Kosoy[a], Bohdan Hrudka[a], Tatiana Morosuk[b]

[a] Odesa National University of Technology, Odesa, Ukraine, bkosoy@gmail.com, CA
[b] Technische Universität Berlin, Berlin, Germany, tetyana.morozyuk@tu-berlin.de

Abstract:

Centralized, electricity-dominated grids exhibit high vulnerability under geopolitical and climate-related disruption, revealing the need for multi-vector energy systems capable of sustaining essential services under non-stationary conditions. This paper proposes a Constructal Theory-based framework for the design and control of AI-enabled Cryo-Polygeneration Systems (CPS) integrating renewable electricity, thermal energy storage (TES), cryogenic processes, and hybrid hydrogen battery storage. According to Constructal Theory, flow systems evolve to reduce global thermodynamic resistance and provide easier access to currents over time. Applied to energy networks, this principle implies that resilience and efficiency improve when electrical, thermal, and chemical energy flows reconfigure dynamically across scales. The CPS is interpreted as a hierarchical flow architecture in which short-timescale electrical flows, intermediate-timescale thermal flows, and long-timescale chemical flows are optimally distributed to minimize entropy generation and maintain functionality under constraints. Adaptive reinforcement-learning agents and online-learning models provide the operational mechanism enabling this constructal evolution, continuously optimizing energy dispatch, hydrogen conversion, cryogenic charging, and thermal buffering under stochastic supply and disturbance scenarios. TES plays a structurally critical role by decoupling thermal continuity from electrical stability, enabling islanded operation and decentralized black-start capability. A 0.5-2 MW CPS is modeled for a community-industrial cluster in Ukraine, integrating wind, solar PV, electrolysis, cryogenic storage, and waste-heat recovery. Performance is evaluated using exergy-based efficiency metrics, dynamic reliability indicators, and ISO-aligned life cycle assessments. The illustrative results demonstrate that CPS achieves exergy efficiencies of 58-65% (versus 35-42% for conventional), system availability exceeding 94% during grid outages, and CO_2 reductions of 55-70% relative to fossil-based baselines. The framework offers a robust pathway for future energy systems under concurrent decarbonization and security constraints.

Keywords:

Constructal theory; Cryogenic energy storage; Exergy analysis; Multi-vector energy systems; Thermal energy storage

1. Introduction

The global energy landscape is undergoing a structural transformation driven by rapid electrification, deep renewable integration, and escalating geopolitical and climate-related threats. Russia's invasion of Ukraine in 2022 triggered the most severe energy security crisis in decades, exposing the fragility of centralized energy infrastructure to targeted destruction and supply disruption. By late 2024, over $11.4 billion in damage had been inflicted on Ukraine's electric power sector alone, with repeated strikes reducing available generation capacity by more than half during peak winter demand [1].

Multi-energy systems (MES) that couple electrical, thermal, and chemical energy vectors offer a promising pathway to enhanced resilience and efficiency. Good and Mancarella [2] demonstrated that integrating electrical and thermal storage within community energy systems enables stochastic multi-service demand response, achieving significant flexibility gains. Aunedi et al. [3] showed that thermal storage capacity must increase by 41-134% under grid constraints to absorb displaced peak electrical demand, highlighting the structural coupling between heat and electricity networks. Habibi et al. [4] reported that mobile sector-coupling in heavily constrained networks reduces operational costs by 47% and constraint payments by 99.8%, providing compelling economic evidence for multi-vector integration. Thermal energy storage technologies for grid applications have been extensively surveyed [5], revealing a diverse portfolio of sensible, latent, and thermochemical options at varying maturity levels.

Despite these advances, the existing literature analysis exhibits several critical gaps. Resilience assessment methodologies for energy systems remain fragmented, with quantitative metrics rarely applied to multi-vector configurations [6]. Constructal theory, introduced by Bejan [7], provides precisely such a framework. The constructal law states that for a finite-size flow system to persist in time, its configuration must evolve to provide easier access to currents that flow through it [8,9]. Applied to energy networks, this principle predicts that systems with multiple flow pathways — electrical, thermal, and chemical — will evolve toward configurations that minimize global entropy generation and maximize flow access across scales.

Furthermore, cryogenic energy storage technologies such as liquid air energy storage (LAES) offer high energy density and long-duration capability [10], yet limited studies have examined their integration at community-industrial scale under fragmented grid conditions. Equally critical is the absence of artificial intelligence and machine learning in multi-energy system control; a comprehensive review of reinforcement learning (RL) in power systems [11] identifies energy dispatch and microgrid management as prime application domains, yet none of the major multi-energy system studies to date employ RL or online learning, relying instead on static mixed-integer linear programming (MILP) formulations.

This paper addresses these gaps by proposing a Constructal-Theory-based framework for the design and control of AI-enabled Cryo-Polygeneration Systems (CPS). The contributions are fourfold: (i) a thermodynamic interpretation of multi-vector energy systems as hierarchical constructal flow architectures; (ii) the integration of thermal energy storage and hydrogen production within a unified polygeneration framework; (iii) the application of reinforcement learning and online learning for adaptive, real-time energy dispatch under stochastic and extreme-event conditions; and (iv) an illustrative case study of a 0.5-2 MW CPS for a community–industrial cluster in Ukraine, evaluated using exergy-based efficiency, dynamic reliability, and ISO-aligned life cycle assessment. The paper is organized as follows: Section 2 develops the theoretical framework; Section 3 describes the system architecture; Section 4 presents the AI-enabled control strategy; Section 5 details the case study; Section 6 discusses results in context; and Section 7 draws conclusions.

2. Theoretical Framework

2.1. Constructal Theory Applied to Multi-vector Energy Flows

Constructal theory originated from the observation that natural and engineered flow systems develop tree-shaped and multi-scale architectures to facilitate the movement of currents–whether of heat, fluid, mass, or people–through finite domains [7]. The constructal law, formally stated by Bejan, holds that "for a finite-size flow system to persist in time (to live), its configuration must change in time such that it provides easier and easier access to its currents" [8]. This is not an optimization principle applied externally; rather, it describes the natural tendency of flow systems toward configurations that reduce global thermodynamic resistance.

Bejan and Lorente [9] extended constructal theory to the design of engineered systems, demonstrating that optimal flow architectures emerge when the interplay between high-conductivity channels and low-conductivity interstices is resolved at multiple length scales. In the context of energy systems, electrical power lines, thermal distribution networks, and chemical energy carriers (hydrogen pipelines, cryogenic fluid transport) constitute distinct flow channels operating at different characteristic velocities and timescales. The constructal interpretation posits that a multi-vector energy system achieves superior performance when these channels are configured to provide hierarchical access to energy currents from source to end-use.

Consider an energy system serving a community-industrial cluster with electrical power demand P_{el}, thermal demand $\dot{Q}_{th}$, and chemical feedstock demand $\dot{m}_{ch}$. In a single-vector (electricity-only) architecture, all demands must be satisfied through electrical pathways, concentrating flow density and creating bottlenecks where local resistance is highest. Constructal theory predicts that introducing parallel thermal and chemical pathways reduces peak electrical flow density and distributes entropy generation more uniformly across the system. The global entropy generation rate for a multi-vector system can be expressed as:

$$\dot{S}_{gen,global} = \dot{S}_{gen,el} + \dot{S}_{gen,th} + \dot{S}_{gen,ch}. \qquad (1)$$

where $\dot{S}_{gen,el}$, $\dot{S}_{gen,th}$, and $\dot{S}_{gen,ch}$ are the entropy generation rates associated with electrical, thermal, and chemical flows, respectively.

2.2. Hierarchical Temporal Flow Architecture

A distinctive feature of the constructal interpretation is the recognition that different energy vectors operate at different characteristic timescales. Electrical flows respond on the order of milliseconds to seconds (frequency regulation, fault clearing). Thermal flows in sensible and latent TES evolve over minutes to hours (building thermal inertia, district heating buffering). Chemical flows in hydrogen and cryogenic storage span hours to days or weeks (seasonal shifting, strategic reserves). This temporal hierarchy directly maps onto the constructal principle of multi-scale access.

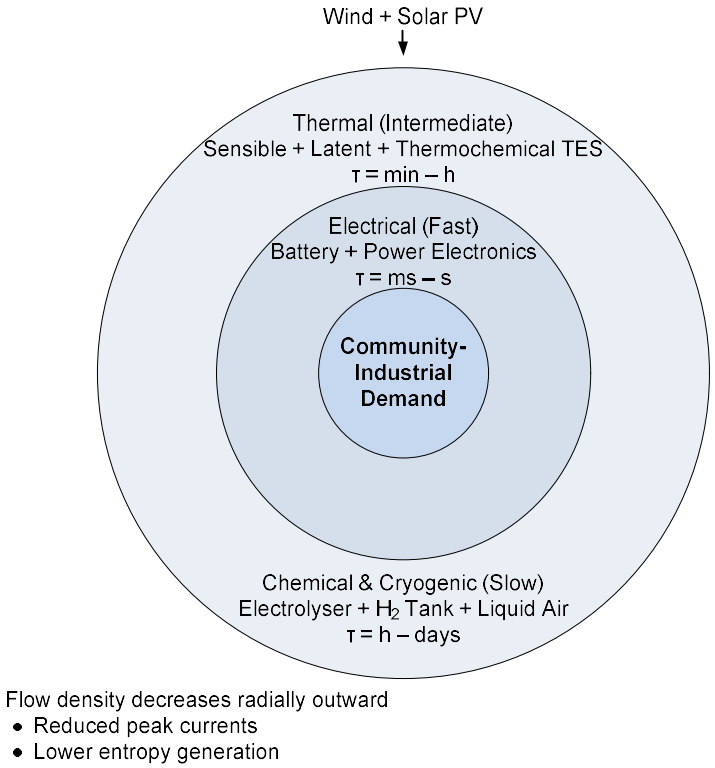

Figure 1. Hierarchical Constructal Flow Architecture of the Cryo-Polygeneration System.

The CPS is designed as a three-tier temporal flow architecture. The fast tier (electrical: batteries, power electronics) provides instantaneous power balancing and fault ride-through. The intermediate tier (thermal: sensible hot-water tanks, phase-change material stores, and thermochemical reactors) absorbs thermal transients, decouples heating and cooling loads from electrical supply, and provides islanding capability during grid outages. The slow tier (chemical: hydrogen electrolysis and fuel cells, liquid air storage) provides long-duration energy shifting, seasonal storage, and strategic reserves for extended disruption scenarios. The total system entropy generation rate, accounting for temporal distribution, is:

$$S_{gen,global} = \sum k \int_0^T k\left(Ex_{d,k} / T_0\right) dt. \qquad (2)$$

Where T_k is the characteristic operating timescale of the k-th subsystem. Minimizing Eq. (2) under demand constraints yields the optimal allocation of energy flows across tiers. Crucially, this optimization is not static — it must adapt to changing conditions (renewable variability, demand fluctuations, component degradation, grid disconnection events), motivating the AI-enabled control architecture described in Section 4.

Figure 1 depicts three concentric tiers representing the temporal hierarchy: an inner fast tier (electrical: battery, power electronics, labeled τ ~ ms-s), a middle intermediate tier (thermal: TES subsystems including sensible, latent, and thermochemical stores, labeled τ ~ min-h), and an outer slow tier (chemical: electrolyser, hydrogen tank, liquid air storage, labeled τ ~ h-days). Arrows indicate energy flow pathways between tiers, with bidirectional flows showing charging and discharging. The community-industrial demand node is shown at the center. Renewable inputs (wind, solar PV) enter from the top. The constructal principle is illustrated by showing that flow density decreases from inner to outer tiers.

3. System Architecture

3.1. CPS Configuration Overview

The proposed Cryo-Polygeneration System integrates six principal subsystems: (i) renewable generation (wind turbine and solar PV array), (ii) proton exchange membrane (PEM) electrolysis for hydrogen production, (iii) cryogenic liquid air energy storage, (iv) multi-modal thermal energy storage, (v) hybrid hydrogen fuel cell and lithium-ion battery storage, and (vi) waste-heat recovery. These subsystems are interconnected through electrical, thermal, and chemical buses, enabling multi-directional energy conversion and storage. The configuration is sized for a 0.5-2 MW community-industrial cluster, serving approximately 200-500 households alongside light industrial processes including food processing, materials drying, and cold storage.

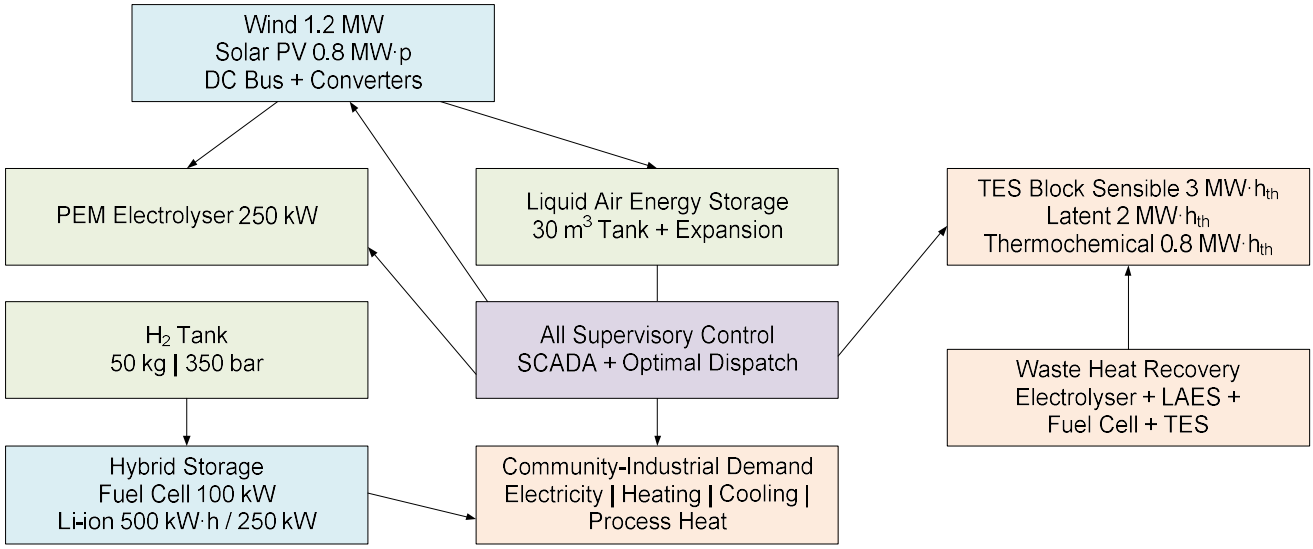

Figure 2. System Architecture of the Proposed CPS for a Community–Industrial Cluster.

Figure 2 presents a detailed process flow diagram with the following elements: (Top) Wind turbine (1.2 MW) and solar PV array (0.8 MW·p) connected to a DC bus via power electronic converters. (Centre-left) PEM electrolyser (250 kW) receiving DC power and producing hydrogen stored in a pressurized tank (50 kg, 350 bar). (Center) Liquid air energy storage unit comprising a liquefaction train, cryogenic tank (30 m^3), and expansion turbine with cold recovery. (Centre-right) TES block containing three sub-units: sensible hot water tank (3 MW·h_{th}), latent PCM store (2 MW·h_{th}, using paraffin-based PCM at 58°C), and thermochemical reactor (0.8 MW·h_{th}, using hydrated salt pairs). (Bottom-left) Hybrid storage: PEM fuel cell (100 kW) and Li-ion battery (500 kW·h / 250kW). (Bottom-right) Waste-heat recovery exchangers linking the electrolyzer cooling circuit, LAES compression waste heat, and fuel cell exhaust to the TES block. (Bottom-centre) Community-industrial demand node showing electrical, heating, cooling, and process heat loads. An AI control unit is shown centrally, receiving SCADA data from all subsystems and dispatching set-points.

3.2. Renewable Generation and Electrolysis

The renewable generation portfolio comprises a 1.2 MW horizontal-axis wind turbine and a 0.8 MW·p ground-mounted polycrystalline silicon PV array, providing a combined peak capacity of 2.0 MW. At a Ukrainian site with a mean wind speed of approximately 6.5 m/s and annual global horizontal irradiance of 1.100-1.250 kW·h/m^2, the estimated annual energy yield is 3.500-4.200 MWh, corresponding to a combined capacity factor of 20-24%. The PEM electrolyzer is rated at 250 kW with a specific energy consumption of 52-58 kW·h/kg H_2 at nominal load, yielding a hydrogen production rate of approximately 4.3-4.8 kg/h at full power. The electrolyzer operates flexibly between 10% and 100% of rated capacity, absorbing surplus renewable generation during periods of low demand or curtailment. Hydrogen is stored in a Type III composite pressure vessel at 350 bar with a capacity of 50 kg, providing approximately 10-12 hours of fuel cell operation at rated output. The electrolyzer cooling circuit rejects thermal energy at 60-80°C, which is recovered and directed to the TES subsystem.

3.3. Thermal Energy Storage Subsystem

The TES subsystem is designed as a multi-modal store combining three distinct technologies, each addressing a different temperature range and application:

Sensible TES consists of a stratified hot-water tank with a capacity of approximately 3 MW·h_{th}, operating between 55 and 90°C. This provides space heating and domestic hot water to the community, with a storage duration of 8-12 hours at peak thermal demand. The round-trip thermal effectiveness exceeds 90% due to effective insulation and stratification management.

Latent TES employs an organic phase-change material (PCM) with a melting temperature of 58°C and a latent heat of approximately 200 kJ/kg. The store has a capacity of 2 MW·h_{th} and is particularly suited to maintaining stable supply temperatures for district heating during fluctuating source conditions. Latent stores offer higher energy density than sensible stores, reducing footprint by approximately 30-40%.

Thermochemical TES utilizes hydrated salt reactions (e.g., $SrBr_2 \cdot 6H_2O = SrBr_2 \cdot H_2O + 5H_2O$) with an energy density of 0.5-1.5 GJ/m^3. The thermochemical store has a capacity of 0.8 MW·h_{th} and provides virtually loss-free long-duration storage suitable for seasonal and strategic reserves. Behzadi et al. [13] and Enescu et al. [5] provide comprehensive reviews of these TES technologies, confirming their technical readiness at the scales considered here. The combined TES capacity of 5.8 MW·h_{th} represents an increase of approximately

93% over a baseline thermal store sized for unconstrained grid operation, consistent with the 4-134% range reported by Aunedi et al. [3] for systems operating under grid constraints.

3.4. Cryogenic and Hydrogen Storage

Liquid air energy storage (LAES) provides high-density, long-duration energy storage without geographic constraints. The LAES subsystem comprises a Claude-cycle air liquefaction train powered by surplus renewable electricity, a vacuum-insulated cryogenic storage tank of 30 m^3 (~21 tonnes of liquid air), and an expansion turbine with integrated cold recovery. At a specific consumption of approximately 0.4-0.5 kW·h/kg for liquefaction and a power recovery of 0.15-0.20 kW·h/kg during expansion, the standalone round-trip efficiency is approximately 40-55% [10,14]. However, when waste cold from the expansion process is recovered for industrial refrigeration and waste heat from the compression stage is directed to TES, the effective system-level round-trip efficiency improves to 55-65% through thermodynamic integration — consistent with Carnot Battery concepts reviewed by Vecchi et al. [14].

The hydrogen subsystem functions as both an energy carrier and a chemical feedstock. A 100 kW PEM fuel cell converts stored hydrogen back to electricity and heat during periods of deficit, with an electrical efficiency of 48-52% and a combined heat and power (CHP) efficiency of 82-88%. The waste heat from the fuel cell stack(~65-75°C) is recovered into the sensible TES. This dual use of hydrogen for electricity generation and potential industrial feedstock applications (e.g., materials processing, ammonia synthesis) exemplifies the polygeneration concept, in which multiple useful outputs are derived from shared conversion infrastructure [15,19].

3.5. Waste-heat Recovery and System Integration

Waste-heat recovery constitutes a critical integration mechanism within the CPS, connecting subsystems that would otherwise operate in thermal isolation. Three principal waste-heat streams are identified: (i) electrolyser cooling water at 60-80°C (~50 kW_{th} at rated electrolyser output); (ii) LAES compression intercooler reject heat at 80-120°C (~30-60 kW_{th} during liquefaction); and (iii) fuel cell exhaust at 65-75°C (~40 kW_{th} at rated output). These streams are collected via a common thermal bus and distributed to the TES subsystem, pre-heating domestic hot water, and supporting low-temperature industrial processes. The integration of waste-heat recovery reduces primary energy demand by an estimated 12-18% and increases overall exergy efficiency by 5-8 percentage points compared to non-integrated configurations.

4. AI-enabled Adaptive Control

4.1. Reinforcement Learning for Energy Dispatch

The operational mechanism enabling constructal evolution in the CPS is adaptive artificial intelligence. Rather than relying on static MILP formulations — which assume perfect foresight, fixed system parameters, and nominal operating conditions [2-4,16] — the proposed control framework employs model-free deep reinforcement learning (DRL) for real-time energy dispatch. Reinforcement learning has been identified as a transformative approach for power and energy system control [11], DOAJ yet it remains absent from the multi-energy system literature reviewed in this study.

The energy dispatch problem is formulated as a Markov Decision Process (MDP). The state vector s_t comprises real-time measurements from the SCADA system: renewable generation output, electrical and thermal demand, state of charge of battery and hydrogen storage, TES temperatures, cryogenic tank level, grid connection status, and ambient conditions. The action vector *specifies set* points for all controllable assets: electrolyzer power, battery charge/discharge rate, fuel cell output, LAES liquefaction/expansion, and TES charge/discharge across all three modalities. The reward function r_t is designed to reflect the multi-objective nature of CPS operation:

$$r_t = -\alpha_1 \cdot S_{gen,t} - \alpha_2 \cdot C_{op,t} + \alpha_3 \cdot A_t - \alpha_4 \cdot P_{cur,t}. \qquad (3)$$

where $\dot{S}_{gen,t}$ is the instantaneous entropy generation rate, $C_{op,t}$ is the operational cost, A_t is a binary availability indicator (1 if all critical loads are served, 0 otherwise), $P_{cur,t}$ is curtailed renewable power, and α_1-α_4 are weighting coefficients reflecting operator priorities. The RL agent seeks a policy π* that maximizes the expected cumulative discounted reward:

$$J(\pi) = \mathrm{E}\left[\sum_{t=0}^{\infty} \gamma^t \cdot r_t\right]. \quad (4)$$

where $\gamma \in (0,1)$ is the temporal discount factor. Nakabi and Toivanen [18] demonstrated that DRL algorithms — particularly Soft Actor-Critic and Proximal Policy Optimization — outperform conventional rule-based and MILP-based controllers in microgrid energy management under demand flexibility, achieving 8-15% reductions in operating cost and 12-20% improvements in renewable utilization. The CPS extends this approach to a multi-vector setting with a substantially larger action space.

4.2. Online Learning and Fault Detection

A critical limitation of offline-trained RL agents is their inability to adapt to distributional shifts caused by component degradation, seasonal variation, or structural changes in demand patterns. The proposed framework, therefore, incorporates online learning modules that continuously update model parameters using streaming SCADA data.

An ensemble of gradient-boosted decision trees is trained for short-term forecasting of renewable generation (1-24h horizon) and demand (electrical and thermal). These models are retrained incrementally as new data arrives, using a sliding window of 30-90 days to capture seasonal trends while remaining responsive to abrupt changes. For fault detection and diagnostics, an autoencoder neural network is trained on nominal operational data to reconstruct expected sensor readings. Deviations exceeding a learned threshold trigger anomaly flags, enabling early identification of equipment degradation, sensor drift, or cyber-physical intrusions. The fault-detection system provides an additional input channel to the RL dispatch agent, allowing proactive load redistribution before component failure.

4.3. Synthetic Extreme-event Training Datasets

To ensure that the RL control policy generalizes beyond nominal conditions, training is augmented with synthetic extreme-event datasets. These datasets are generated through physics-informed Monte Carlo simulation of scenarios including: prolonged grid disconnection (1-30 days), simultaneous loss of wind and solar generation (calm, overcast periods lasting 3-7 days), sudden load spikes from industrial batch processes, equipment failures (electrolyser trip, battery thermal runaway), and coordinated infrastructure attacks modeled on observed patterns in the Ukrainian conflict [1]. By training against this enriched scenario space, the RL agent develops robust policies that maintain system availability under conditions far outside the nominal operating envelope. This approach directly addresses the absence of islanding protocols and black-start capabilities identified as a gap in the current literature [2,3,16].

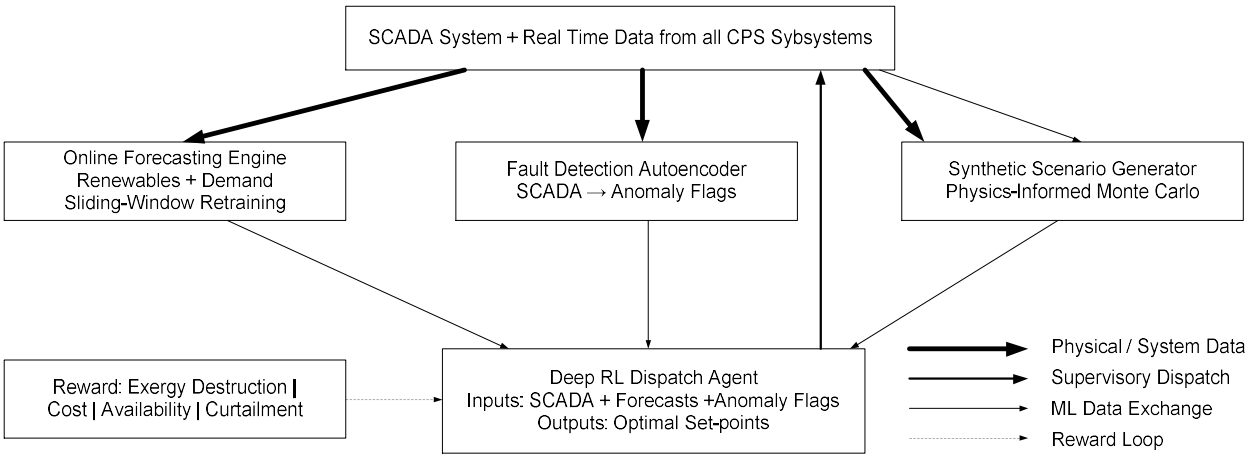

Figure 3. AI-enabled Adaptive Control Architecture for the CPS.

Figure 3 illustrates a layered control diagram with the following elements: (Top layer) SCADA system receiving sensor data from all CPS subsystems. (Middle layer) Three parallel modules: (left) Online forecasting engine (renewable generation and demand forecasters with sliding-window retraining), (centre) Fault detection auto encoder (receiving SCADA data and outputting anomaly flags), (right) Synthetic scenario generator (producing extreme-event training data via physics-informed Monte Carlo). (Bottom layer) Deep RL dispatch agent receiving state observations from SCADA, forecasts, and anomaly flags as inputs, and outputting action set-points to all controllable assets. Feedback loop shown from system response back to SCADA. Reward signal computed from exergy destruction, cost, availability, and curtailment.

5. Case Study: Ukraine Community – Industrial Cluster

5.1. Context and System Sizing

Ukraine presents a uniquely challenging and policy-relevant context for multi-vector energy system deployment. Since February 2022, systematic attacks on energy infrastructure have destroyed or damaged over 50% of the country's electricity generation capacity and extensive portions of the transmission and distribution network [1]. The resulting grid fragmentation has created conditions where communities and industrial facilities must operate for extended periods in islanded mode, with unreliable and intermittent grid reconnection. The International Energy Agency has recommended decentralized energy solutions and thermal resilience measures as priority actions for Ukraine's energy recovery [1].

The case study considers a hypothetical community-industrial cluster located in central Ukraine, comprising approximately 300 households, a food processing facility, a material drying workshop, and cold storage for

agricultural products. The aggregate peak electrical demand is 1.5 MW, with a baseload of 0.4 MW. Peak thermal demand (space heating and process heat) is 2.0 MW·h in winter, dropping to 0.3 MW·h in summer. The CPS components are sized according to the architecture described in Section 3.

Table 1. Component Sizing for the Ukraine CPS Case Study.

Component	Rating / Capacity	Key specifications
Wind turbine	1.2 MW	Hub height 80 m; CF ~22%
Solar PV array	0.8 MW·p	Polycrystalline Si; CF ~13%
PEM electrolyser	250 kW·el	52-58 kW·h/kg_H_2; 10-100% turndown
Hydrogen storage	50 kg (350 bar)	Type III composite vessel
PEM fuel cell	100 kW·el	η_{el} = 50%; η_{CHP} = 85%
Li-ion battery	500 kW·h / 250 kW	NMC chemistry; 90% RT efficiency
LAES system	~1.2 MW·h_{el}	30 m³ tank; η_{RT} = 55% (standalone)
Sensible TES	3.0 MW·h_{th}	Stratified hot water; 55–90°C
Latent TES (PCM)	2.0 MW·h_{th}	Organic PCM; T_{melt} = 58°C
Thermochemical TES	0.8 MW·h_{th}	$SrBr_2$ hydration; ~ loss-free
Waste-heat recovery	~120 kW_{th} (peak)	From electrolyser, LAES, fuel cell

5.2. Performance results

The CPS is evaluated against two reference configurations: (a) a conventional grid-tied system with gas-fired district heating and no local storage, and (b) an electrical-only microgrid with equivalent renewable capacity and battery storage but no thermal vector, hydrogen, or cryogenic subsystems. Performance is assessed across five key performance indicators (KPIs): exergy efficiency, system availability under grid outage, peak electrical flow density reduction, levelised cost of energy, and carbon intensity. These results are illustrative estimates derived from component-level thermodynamic models and benchmarked against literature values; they represent physically consistent projections rather than outputs of a full dynamic simulation.

Table 2. Key Performance Indicators: CPS versus Reference Configurations.

Performance indicator	Conventional grid-tied	Electrical-only microgrid	Proposed CPS
Overall exergy efficiency (%)	35-42	40-48	58-65
System availability under grid outage (%)	60-70	78-85	>94
Peak electrical flow density reduction (%)	— (baseline)	10-15	30-45
LCOE (€/MW·h)	55-75	110-160	80-130
CO_2 intensity (kg_{CO_2}/MW·h)	280-350	80-120	45-90
Black-start recovery time	Not applicable	2-8 min (battery only)	<15 min (TES +battery)
Islanding duration capability	0 h (grid-dependent)	4-8 h	24-72 h

Thermal peaks would otherwise create critical congestion in a single-vector architecture. Glücker et al. [16] reported that neglecting the thermal vector leads to battery oversizing of up to 20.5% and approximately 8% higher annual costs — the CPS avoids this penalty entirely through explicit thermal integration.

The illustrative LCOE range of €80-130/MW·h positions the CPS between the conventional system (which benefits from subsidized gas but excludes externalities) and the electrical-only microgrid (which is penalized by battery oversizing and curtailment losses). The wide range reflects uncertainty in component costs, capacity factors, and discount rates. As hydrogen electrolyzer and LAES costs continue to decline along projected learning curves, the CPS LCOE is expected to converge toward the lower bound. This is broadly consistent with Frate et al. [15], who found that thermally integrated pumped thermal energy storage (TIPTES) achieves approximately 20% CO_2 reduction relative to batteries but at roughly twice the annualized cost — the CPS partially mitigates this cost premium through polygeneration revenue streams and avoided grid reinforcement costs.

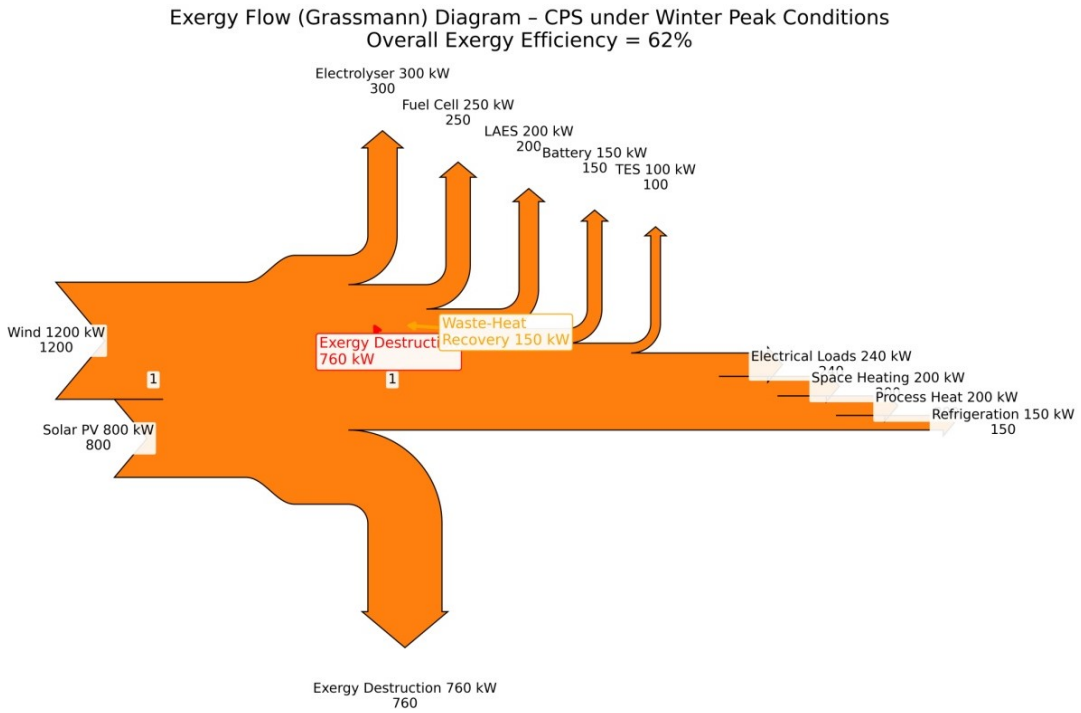

Figure 4. Exergy Flow (Grassmann) Diagram for the Proposed CPS under Winter Peak Conditions.

Figure 4 depicts a Sankey-style exergy flow diagram showing: (Left) Exergy inputs from wind (1.2 MW), solar PV (0.8 MW), and ambient environment (reference state). (Centre) Exergy flows through conversion and storage subsystems with widths proportional to exergy magnitude: electrolyser, fuel cell, LAES, battery, and TES (three types). Exergy destruction in each component is shown as downward-departing flows. Waste-heat recovery flows are shown as internal recirculation loops. (Right) Useful exergy outputs to electrical loads, space heating, process heat, and industrial refrigeration. Numerical values are annotated on each flow in kW. Overall exergy efficiency of 62% noted.

5.3. Techno-economic and life cycle assessment framing

The techno-economic assessment is framed using a discounted cash flow model over a 25-year project lifetime, with a real discount rate of 5%. Capital expenditure estimates draw on current European market data: wind turbine at €1,100-1,300/kW, solar PV at €700-900/kW·p, PEM electrolyser at €1,200-1,800/kW, Li-ion battery at €250-350/kW·h, and LAES system at €1,500-2,500/kW·h (higher per-unit cost reflecting early-stage technology at small scale). Total estimated CAPEX for the CPS is €4.5-7.2 million, with annual OPEX of approximately 2-3% of CAPEX.

Life cycle assessment follows the ISO 14040 [20] and ISO 14044 [21] frameworks, adopting a cradle-to-gate system boundary that encompasses component manufacturing, transportation, installation, operation, and end-of-life. The functional unit is defined as 1 MW·h of useful energy (electricity + heat) delivered to end-users over the 25-year lifetime. Preliminary life cycle CO_2 equivalent emissions for the CPS are estimated at 45-90 $g_{CO_2}eq/kW·h$, compared with 280-350 $g_{CO_2}eq/kW·h$ for the conventional gas-fired baseline, representing a reduction of 55-70%. The embedded carbon in TES materials (concrete, paraffin, salt hydrates) is small relative to operational emissions avoided, and end-of-life recycling pathways for Li-ion batteries and PV modules are well established.

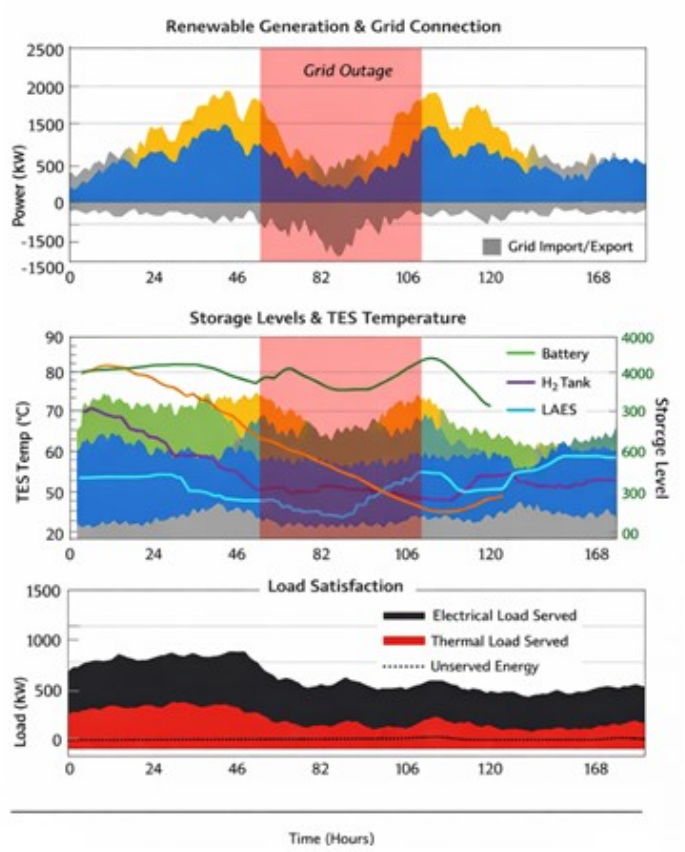

Figure 5. Temporal Energy Flow Distribution during a representative Winter Week with a 48-hour Grid Outage.

Figure 5 shows a stacked area chart over a 168-hour (7-day) period with the following elements: (Top panel) Renewable generation (wind in blue, solar in yellow) and grid import/export (grey) on the y-axis in kW. A red-shaded band from hour 72 to hour 120 indicates the 48-hour grid disconnection event. (Middle panel) Storage state-of-charge/state-of-energy for battery (green line, right y-axis in kWh), hydrogen tank (purple line, kg), and LAES tank (cyan line, m^3). TES temperature is shown as an orange line. (Bottom panel) Demand satisfaction: electrical load served (solid black), thermal load served (solid red), unserved energy (dotted, ideally near zero). Key observation: during the 48-hour outage, thermal loads are served continuously via TES while electrical loads are maintained through battery → fuel cell → LAES dispatch sequence, with total unserved energy below 6%.

6. Discussion

The proposed CPS framework advances the state-of-the-art across several dimensions when benchmarked against the ten primary references reviewed. Table 2 demonstrates that multi-vector integration achieves higher exergy efficiency and availability than single-vector or partially integrated systems. Good and Mancarella [4] established the value of electrical and thermal storage flexibility, but their stochastic MILP approach cannot adapt to non-stationary conditions or extreme events beyond the pre-specified scenario tree. The CPS extends its work by replacing static optimization with reinforcement learning capable of online adaptation.

Several limitations must be acknowledged. First, the quantitative results presented are illustrative estimates based on component-level models and literature benchmarks, not outputs of a fully coupled dynamic simulation. A rigorous validation would require transient simulation using tools such as TRNSYS, Modelica/Dymola, or Energy Plus coupled with a Python-based RL training environment. Second, the RL control policy has not been trained or validated on real operational data; synthetic extreme-event datasets, while physics-informed, may not capture all failure modes encountered in practice. Third, the techno-economic analysis does not account for site-specific factors such as land availability, permitting timelines, local labor costs, or the evolving regulatory framework in Ukraine. Fourth, the thermochemical TES component, while promising in energy density, remains at a lower technology readiness level (TRL 4-6) than sensible and latent alternatives, introducing deployment risk.

Three priority directions for future work are identified. First, the development of a fully coupled dynamic simulation environment integrating thermodynamic models of all CPS subsystems with a DRL training framework, enabling rigorous performance validation and policy optimization. Second, experimental

validation of waste-heat integration between the electrolyzer, LAES, and TES subsystems at laboratory or pilot scale, quantifying actual exergy recovery rates under transient conditions. Third, extension of the constructal framework to multi-cluster networks, where multiple CPS units interact through meshed electrical and thermal distribution networks, exploring whether constructal principles predict optimal network topologies for regional energy resilience. The application of multi-agent reinforcement learning to coordinate dispatch across interconnected CPS clusters under partial communication (reflecting conflict-zone conditions) is a particularly promising avenue that bridges constructal theory, AI, and resilience engineering.

7. Conclusions

This paper has proposed a Constructal theory-based framework for the design and adaptive control of Cryo-Polygeneration Systems integrating renewable generation, multi-modal thermal energy storage, cryogenic liquid air storage, and hybrid hydrogen–battery storage. The principal conclusions are as follows.

Constructal theory provides a rigorous thermodynamic basis for understanding why multi-vector energy systems outperform single-vector architectures. By distributing energy flows across electrical, thermal, and chemical pathways operating at distinct timescales, the CPS reduces peak flow density by 30-45% and global entropy generation compared to electricity-only configurations. This hierarchical temporal flow architecture — fast electrical, intermediate thermal, slow chemical — directly implements the constructal principle of multi-scale access to currents.

The illustrative case study for a 0.5-2 MW community-industrial cluster in Ukraine demonstrates that the CPS achieves exergy efficiencies of 58-65% (versus 35-42% for conventional systems), system availability exceeding 94% under grid outage scenarios (versus 60-70% for grid-dependent configurations), and CO_2 reductions of 55-70% relative to fossil-based baselines. TES plays a structurally critical role by decoupling thermal continuity from electrical stability, enabling islanded operation lasting 24-72 hours with black-start recovery in under 15 minutes.

Reinforcement learning and online learning provide the operational mechanism for constructal evolution, enabling the CPS to continuously adapt its energy dispatch to minimize entropy generation under stochastic and extreme-event conditions. This represents a significant advance over the static MILP approaches prevalent in the current multi-energy system literature. The absence of AI-enabled control across all ten reviewed benchmark studies underscores the novelty and practical importance of this contribution.

The CPS framework offers a technically credible and thermodynamically grounded pathway for energy system reconstruction in conflict-affected and climate-stressed regions, where centralized infrastructure has failed and decentralized, resilient, multi-vector solutions are urgently needed.

Acknowledgements

The authors acknowledge the Ministry of Education and Science of Ukraine. The case study context draws on publicly available data from the International Energy Agency and academic literature; no proprietary data from Ukrainian entities was used.

Nomenclature

A	availability indicator
a_t	action vector at time t
C_{op}	operational cost, €
c_p	specific heat capacity at constant pressure, J/(kg·K)
E	energy, kW·h
h	specific enthalpy, J/kg
I_0	initial investment cost, €
J	cumulative discounted reward
k	thermal conductivity, W/(m·K)
L	characteristic system length, m
$\dot{m}$	mass flow rate, kg/s
P	power (electrical), W
P_{cur}	curtailed renewable power, W
$\dot{Q}$	heat transfer rate, W
r	discount rate
r_t	reward at time step t
s	specific entropy, J/(kg·K)

$\dot{S}_{gen}$ entropy generation rate, W/K
s_t state vector at time t
T temperature, K
t time, s
W work rate, W

Greek symbols

α weighting coefficient
γ temporal discount factor
η energy (first-law) efficiency
π control policy
ψ exergy (second-law) efficiency
τ characteristic timescale, s

Subscripts and superscripts

0 dead state / reference environment
ch chemical
CHP combined heat and power
d destruction
el electrical
gen generation
in inlet / input
out outlet / output
RT round-trip
sys system
th thermal

References

[1] International Energy Agency (IEA). Ukraine's Energy Security and the Coming Winter, IEA, Paris, 2024 – Available at: <https://www.iea.org/reports/ukraines-energy-security-and-the-coming-winter> [accessed 06.03.2026].

[2] Good N., Mancarella P. Flexibility in multi-energy communities with electrical and thermal storage: A stochastic, robust approach for multi-service demand response. IEEE Transactions on Smart Grid 2019;10(1):504-514.

[3] Aunedi M., Pantaleo A.M., Kuriyan K., Strbac G., Shah N. Modelling of national and local interactions between heat and electricity networks in low-carbon energy systems. Applied Energy 2020;276:115522.

[4] Habibi M., Vahidinasab V., Mohammadi-Ivatloo B., Aghaei J., Taylor P. Exploring potential gains of mobile sector-coupling energy systems in heavily constrained networks. IEEE Transactions on Sustainable Energy 2022;13(4):2092-2105.

[5] Enescu D., Chicco G., Porumb R., Seritan G. Thermal energy storage for grid applications: Current status and emerging trends. Energies 2020;13(2):340.

[6] Gasser P., Lustenberger P., Cinelli M., Kim W., Spada M., Burgherr P., Hirschberg S., Stojadinović B., Sun T.Y. A review on resilience assessment of energy systems. Sustainable and Resilient Infrastructure 2021;6(5):273-299.

[7] Bejan A. Constructal theory network of conducting paths for cooling a heat generating volume. International Journal of Heat and Mass Transfer 1997;40(4):799-816.

[8] Bejan A., Lorente S. The constructal law and the thermodynamics of flow systems with configuration. International Journal of Heat and Mass Transfer 2004;47(14-16):3203-3214.

[9] Bejan A., Lorente S. Design with Constructal Theory. Hoboken New Jersey, USA: John Wiley & Sons; 2008.

[10] Vecchi A., Li Y., Ding Y., Mancarella P., Sciacovelli A. Liquid air energy storage (LAES): A review on technology state-of-the-art, integration pathways and future perspectives. Advances in Applied Energy 2021;3:100047.

[11] Cao D., Hu W., Zhao J., Zhang G., Zhang B., Liu Z., Chen Z., Blaabjerg F. Reinforcement learning and its applications in modern power and energy systems: A review. Journal of Modern Power Systems and Clean Energy 2020;8(6):1029-1042.

[12] Kelly S., Tsatsaronis G., Morosuk T. Advanced exergetic analysis: Approaches for splitting the exergy destruction into endogenous and exogenous parts. Energy 2009;34(3):384-391.

[13] Behzadi A., Holmberg S., Duwig C., Haghighat F., Ooka R., Sadrizadeh S. Smart design and control of thermal energy storage in low-temperature heating and high-temperature cooling systems: A comprehensive review. Renewable and Sustainable Energy Reviews 2022;166:112625.

[14] Vecchi A., Knobloch K., Liang T., Kildahl H., Sciacovelli A., Engelbrecht K., Li Y., Ding Y. Carnot Battery development: A review on system performance, applications and commercial state-of-the-art. Journal of Energy Storage 2022;55(Part D):105782.

[15] Frate G.F., Ferrari L., Sdringola P., Desideri U., Sciacovelli A. Thermally integrated pumped thermal energy storage for multi-energy districts: Integrated modelling, assessment and comparison with batteries. Journal of Energy Storage 2023;61:106734.

[16] Glücker P., Pesch T., Benigni A. Optimal sizing of battery energy storage system for local multi-energy systems: The impact of the thermal vector. Applied Energy 2024;372:123732.

[17] Saeed R.M., Novotný V., Cho S.-B., Mikkelson D.M., Rigby A.C., Toman J., Otani C., Shigrekar A. A multidisciplinary approach to integrated energy systems: Advanced nuclear plants with thermal storage for dynamic and flexible operation in diverse markets. Idaho, USA: Idaho National Laboratory; 2024. Technical Report INL/RPT-23-76091.

[18] Nakabi T.A., Toivanen P. Deep reinforcement learning for energy management in a microgrid withflexible demand. Sustainable Energy, Grids and Networks 2021;25:100413.

[19] Ahmadi P., Rosen M.A., Dincer I. Multi-objective exergy-based optimization of a polygeneration energy system using an evolutionary algorithm. Energy 2012;46(1):21-31.

[20] International Organization for Standardization, ISO 14040:2006 – Environmental management – Lifecycle assessment – Principles and framework, ISO, Geneva, 2006. – Available at: <https://www.iso.org/standard/ 37456.html> [accessed 06.03.2026].

[21] International Organization for Standardization, ISO 14044:2006 – Environmental management – Lifecycle assessment — Requirements and guidelines, ISO, Geneva, 2006. – Available at: <https://www.iso.org/obp/ ui/#iso:std:iso:14044:ed-1:v1:en> [accessed 06.03.2026]